Glacial-to-interglacial changes in nitrate supply and consumption in the subarctic North Pacific from microfossil-bound N isotopes at two trophic levels

Haojia Ren[1,2], Anja S. Studer[3,4], Sascha Serno[2,5], Daniel M. Sigman[3], Gisela Winckler[2,6], Robert F. Anderson[2,6], Sergey Oleynik[3], Rainer Gersonde[7], and Gerald H. Haug[4]

[1]Department of Geosciences, National Taiwan University, Taipei, Taiwan, [2]Lamont-Doherty Earth Observatory, Columbia University, Palisades, New York, USA, [3]Department of Geosciences, Princeton University, Princeton, New Jersey, USA, [4]Geological Institute, ETH Zurich, Zurich, Switzerland, [5]DFG-Leibniz Center for Surface Process and Climate Studies, Institute of Earth and Environmental Science, University of Potsdam, Potsdam-Golm, Germany, [6]Department of Earth and Environmental Sciences, Columbia University, New York, New York, USA, [7]Alfred Wegener Institute for Polar and Marine Research, Bremerhaven, Germany

Abstract Reduced nitrate supply to the subarctic North Pacific (SNP) surface during the last ice age has been inferred from coupled changes in diatom-bound $\delta^{15}N$ (DB-$\delta^{15}N$), bulk sedimentary $\delta^{15}N$, and biogenic fluxes. However, the reliability of bulk sedimentary and DB-$\delta^{15}N$ has been questioned, and a previously reported $\delta^{15}N$ minimum during Heinrich Stadial 1 (HS1) has proven difficult to explain. In a core from the western SNP, we report the foraminifera-bound $\delta^{15}N$ (FB-$\delta^{15}N$) in *Neogloboquadrina pachyderma* and *Globigerina bulloides*, comparing them with DB-$\delta^{15}N$ in the same core over the past 25 kyr. The $\delta^{15}N$ of all recorders is higher during the Last Glacial Maximum (LGM) than in the Holocene, indicating more complete nitrate consumption. *N. pachyderma* FB-$\delta^{15}N$ is similar to DB-$\delta^{15}N$ in the Holocene but 2.2‰ higher during the LGM. This difference suggests a greater sensitivity of FB-$\delta^{15}N$ to changes in summertime nitrate drawdown and $\delta^{15}N$ rise, consistent with a lag of the foraminifera relative to diatoms in reaching their summertime production peak in this highly seasonal environment. Unlike DB-$\delta^{15}N$, FB-$\delta^{15}N$ does not decrease from the LGM into HS1, which supports a previous suggestion that the HS1 DB-$\delta^{15}N$ minimum is due to contamination by sponge spicules. FB-$\delta^{15}N$ drops in the latter half of the Bølling/Allerød warm period and rises briefly in the Younger Dryas cold period, followed by a decline into the mid-Holocene. The FB-$\delta^{15}N$ records suggest that the coupling among cold climate, reduced nitrate supply, and more complete nitrate consumption that characterized the LGM also applied to the deglacial cold events.

1. Introduction

During the Pleistocene ice ages, the subarctic North Pacific (SNP) and the Antarctic, on nearly opposite sides of the Earth, were both characterized by low productivity as indicated by low burial fluxes of biogenic components and low surface nitrate concentration as indicated by nitrogen isotopic data [*François et al.*, 1997; *Sigman et al.*, 1999; *Robinson et al.*, 2004; *Brunelle et al.*, 2007, 2010; *Robinson and Sigman*, 2008]. Looking further back in time, the onset of major ice age cycles approximately 2.7 million years ago also coincided with a sharp drop in productivity and stable or increased surface nitrate consumption in the SNP and Antarctic [*Haug et al.*, 1999; *Sigman et al.*, 2004; *Studer et al.*, 2012]. These coupled changes have been explained by reduced supply of nitrate into the sunlit surface layer of both polar regions, due to stronger density stratification of the upper water column [*Sigman et al.*, 2004] and/or a weakening in the physical drivers of vertical water exchange, such as the westerly winds [*Toggweiler et al.*, 2006; *Anderson et al.*, 2009]. Below, simply as a shorthand, we refer to the reduced surface/deep exchange of water implied by the reduced gross nitrate supply as "stratification."

During ice ages, stratification in the Antarctic zone of the Southern Ocean may have reduced deep ocean ventilation [*François et al.*, 1997; *Sigman et al.*, 1999; *Anderson et al.*, 2009]. By decreasing the upwelling of carbon dioxide-rich deep water and the pumping of unused dissolved nutrients back into the deep ocean, this may have driven a substantial part of the reduction in atmospheric CO_2 content during ice ages

[*Hain et al.*, 2010]. In contrast, with no deep water formation in the SNP today, ice age stratification in the SNP is less likely to have played an important role in ventilation of the deep ocean or in ice age CO_2 reduction, as there was no deep ocean ventilation by the SNP to reduce during ice ages.

Nevertheless, the SNP provides a helpful test case for understanding the response of halocline-bearing polar regions to climate change. This is aided by the fact that the SNP hosts adequate burial of foraminifera for the established tools of paleoceanography to be applied in this region, in contrast to the notoriously $CaCO_3$-poor Antarctic. Moreover, the SNP hosts very important fisheries and affects climate in the northern continents, additional motivations for understanding the response of this ocean region to climate change.

The similar paleobiogeochemical behavior of the Antarctic and SNP over glacial/interglacial cycles is somewhat surprising, given that the two regions have very different boundary conditions. While both regions experience net Ekman divergence, the southern westerly winds and the Antarctic Circumpolar Current are largely unimpeded by continental barriers, in contrast to the winds and currents of the North Pacific. Moreover, as described above, the vertical density structure of the two regions has very different outcomes for deep ocean ventilation by the two regions, with the Antarctic forming both intermediate and deep water and the SNP forming only intermediate water [*Talley et al.*, 2011]. Given these differences, it would seem possible to hone in on their shared aspects to identify a physical explanation for the apparent reduction in surface/deep exchange during cold climate that appears to characterize both regions.

However, a number of aspects of the deglacial histories in the subarctic North Pacific complicate the picture. In the SNP, the dramatic increase in biogenic fluxes occurred at the Bølling/Allerød (B/A, 14.6 ka) warm period [*Crusius et al.*, 2004; *Brunelle et al.*, 2007, 2010; *Jaccard et al.*, 2009; *Kohfeld and Chase*, 2011], which in itself could be consistent with the argued glacial/interglacial correlation of increased surface/deep exchange with warm climate. However, the $\delta^{15}N$ of diatom-bound and bulk sedimentary N declines prior to this, at the beginning of Heinrich Stadial 1 (HS1) at ~17.5 ka, prior to the B/A rise in biogenic fluxes, and $\delta^{15}N$ rises back to near-glacial values in the B/A just as opal flux rises [*Brunelle et al.*, 2007, 2010; *Jaccard et al.*, 2009; *Studer et al.*, 2013], which would appear to argue for a rise in the degree of nitrate consumption upon regional warming [*Lam et al.*, 2013]. In short, the specific timing of SNP $\delta^{15}N$ changes across the deglaciation has suggested departures from the overturning-driven $\delta^{15}N$/productivity anticorrelation that characterizes overall glacial/interglacial changes in both the SNP and the Antarctic. Moreover, benthic/planktic radiocarbon comparison has been used to suggest that there was direct ventilation of the deep ocean from the North Pacific surface during HS1, potentially contributing to the first pulse of deglacial atmospheric CO_2 rise [*Okazaki et al.*, 2010; *Rae et al.*, 2014]. This argument appears to be consistent with existing diatom-bound $\delta^{15}N$ (DB-$\delta^{15}N$) records from the open SNP and Bering Sea [*Brunelle et al.*, 2007, 2010], which suggest decreased nitrate consumption and thus potentially increased surface/deep exchange during the HS1 cold period.

Two factors have been suggested as possible sources of complication in N isotopic studies of the SNP, potentially biasing our understanding deglacial change in the region. First, there are dramatic shallow suboxic events in the Bering Sea and the eastern North Pacific during the B/A and after the Younger Dryas (YD) cold interval [*Cannariato and Kennett*, 1999; *Cook et al.*, 2005], apparently associated with a general intensification of suboxia along the eastern North Pacific margin [*Zheng et al.*, 2000], and these are associated with bulk sediment $\delta^{15}N$ maxima in margin sediments where neither variable nitrate consumption nor diagenesis should be major factors [*Chang et al.*, 2008; *Addison et al.*, 2012]. This suggests that the $\delta^{15}N$ of the subsurface nitrate being mixed or upwelled into the SNP euphotic zone was elevated during the B/A and post-YD intervals. However, it is not clear whether these signals propagated into the western SNP, where vigorous wintertime mixing may penetrate through and thus erode such a nitrate $\delta^{15}N$ maximum in the shallow subsurface.

Second, the concentration and chemical characteristics of opal vary downcore in SNP sediments [*Ren et al.*, 2013], with a lower concentration in the clay-rich glacial sediments and particularly low concentration in the Heinrich Stadial 1 (HS1) interval [*Keigwin et al.*, 1992; *Jaccard et al.*, 2009; *Brunelle et al.*, 2010]. To address questions regarding diatom-bound N isotopes and the low $\delta^{15}N$ observed during the HS1 event, size-fractionated opal-bound $\delta^{15}N$ analyses were undertaken [*Studer et al.*, 2013]. The results indicate that the low $\delta^{15}N$ of HS1 may be an artifact of contamination by sponge spicules, which have a very low $\delta^{15}N$ in these sediments (~−11‰) and which are proportionally more important in the sediments with the lowest diatom concentrations [*Studer et al.*, 2013]. However, as yet, we do not have the capability, using opal-based data alone, to either robustly quantify this artifact or remove it.
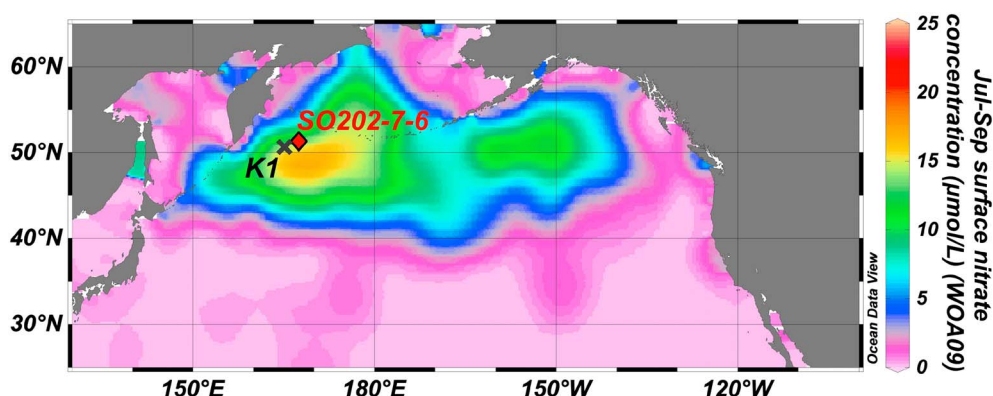
Figure 1. Map showing the summer surface nitrate concentration in the North Pacific (WOA09) [*García et al.*, 2010]. The locations for the core site SO202-7-6 and hydrostation K1 are indicated with a red diamond and a black cross, respectively.

Foraminifera-bound $\delta^{15}N$ (FB-$\delta^{15}N$) analysis was first developed for studies in low-latitude, carbonate-rich sediments [*Ren et al.*, 2009, 2012a; *Meckler et al.*, 2011; *Straub et al.*, 2013a] but is proving equally promising in high-latitude regions when adequate foraminifera are available [e.g., *Straub et al.*, 2013b; *Martínez-García et al.*, 2014]. The two broadly encountered polar to subpolar species are *Neogloboquadrina pachyderma* (sinistral, or left coiling), a nonspinose, asymbiotic form, and *Globigerina bulloides*, a spinose, asymbiotic form. The available data indicate that both species track the $\delta^{15}N$ of nitrate consumed by phytoplankton in the upper ocean, with species-specific offsets [*Ren et al.*, 2012b; *Straub et al.*, 2013b]. In sediments where both diatom opal and foraminifera are adequately abundant for analysis, each component has its advantages and disadvantages. Among the advantages of foraminifera relevant for the standing questions regarding the SNP are that they can be unambiguously separated from nonforaminifera material and sorted by species. Of course, combining data from both components has the potential to provide additional biogeochemical insight.

To more definitively address both Last Glacial Maximum (LGM)-to-Holocene and deglacial $\delta^{15}N$ changes in the SNP, we generated microfossil-bound N isotope measurements of planktonic foraminifera in the same sediment record that *Studer et al.* [2013] investigated for diatom-bound $\delta^{15}N$, with measurements spanning from the LGM to mid-Holocene to late Holocene. The result of combining all the fossil-bound $\delta^{15}N$ data is a self-consistent picture of the connection between climate and the degree of nitrate consumption in the western SNP.

2. Materials and Methods

2.1. Sediment Core and Stratigraphy

Sediment core SO202-07-6 was retrieved from Detroit Seamount in the NW subarctic Pacific during the Innovative North Pacific Experiment (INOPEX) cruise in 2009 (Figure 1; 51.3°N, 167.7°E, 2345 m water depth) [*Gersonde*, 2012]. The age model is based on a high-resolution planktonic foraminiferal radiocarbon stratigraphy measured on *N. pachyderma* (sinistral), with further tuning by tying deglacial features in the high-resolution ^{230}Th-normalized terrestrial ^{4}He (^{4}He$_{terr}$) flux record from SO202-07-6 to abrupt changes in the dust record from NorthGRIP (NGRIP) [*Serno et al.*, 2015]. The sedimentation rate at this site varies between 2 and 7 cm/kyr in the intervals of 27,359–15,197 years B.P. and 11,004–3894 years B.P. and is higher, ~7–20 cm/kyr, between 15,197 and 11,004 years B.P. For additional paleoceanographic context, the calcite $\delta^{18}O$ of the benthic foraminifera *Uvigerina peregrina* was measured in the Stable Isotope Laboratory at Lamont-Doherty Earth Observatory (LDEO) (Table S1 in supporting information). Between 50 and 80 μg of whole foraminifera was analyzed for $\delta^{18}O$ on a Thermo Delta V+ Dual Inlet mass spectrometer connected to a Kiel IV carbonate reaction device at LDEO. The NBS-19 standard was analyzed five to six times daily and indicated a long-term precision of ±0.06‰ for $\delta^{18}O$.

2.2. N Isotope Analyses

The measurements of microfossil-bound $\delta^{15}N$ use the "persulfate-denitrifier" technique [*Knapp et al.*, 2005]. The protocol includes (1) chemical treatment of the microfossil to remove external contaminants, (2) conversion of the organic nitrogen bound within the microfossil walls to nitrate by persulfate oxidation
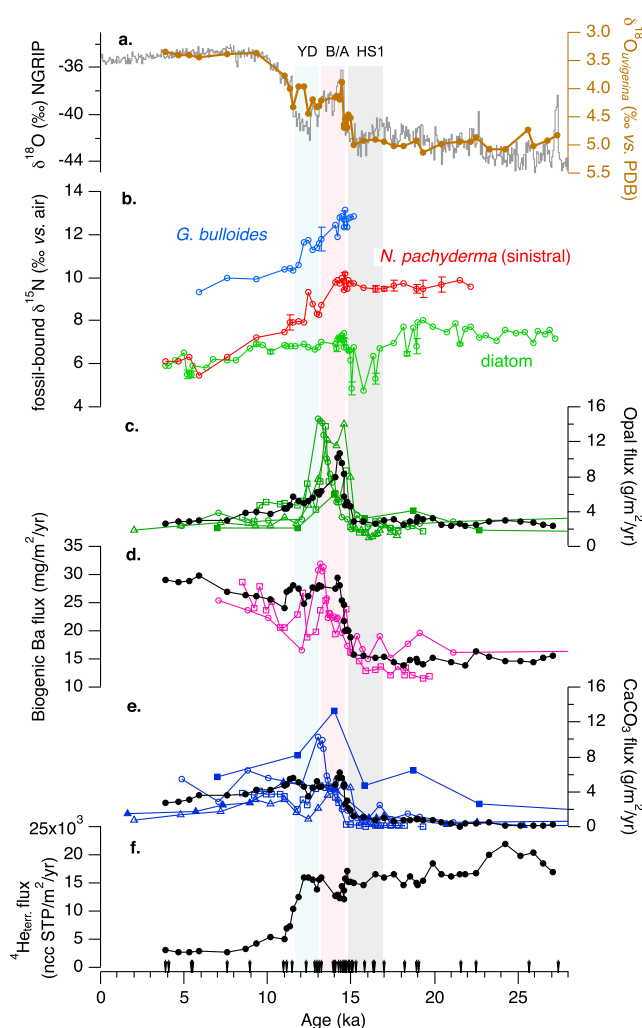
Figure 2. (a) The calcite δ^{18}O of *Uvigerina peregrina* (brown) at SO202-07-6 plotted together with the NGRIP δ^{18}O [*NGRIP members*, 2004]. (b) FB-δ^{15}N of *N. pachyderma* (red) and *G. bulloides* (blue) and DB-δ^{15}N (green) over the last 27 kyr at SO202-07-6. Error bars represent the standard deviations for full cleaning-persulfate-denitrifier replicates as described in the methods. (c–e) ^{230}Th-normalized opal fluxes, biogenic Ba fluxes, and carbonate fluxes from SO202-07-6 (filled circle and highlighted in black) (Serno et al., in preparation) and from published records in the northwest Pacific (RAMA44PC [*Crusius et al.*, 2004] (open triangle), ODP882 [*Jaccard et al.*, 2009] (open square), and PC13 [*Brunelle et al.*, 2010] (open circle)) and in the Bering Sea (RC10-196 [*Kohfeld and Chase*, 2011] (filled square) and JPC17 [*Brunelle et al.*, 2007] (filled triangle)). (f) The ^{4}He$_{terr}$ flux at SO202-7-6 [*Serno et al.*, 2015]. The black arrows along the *x* axis indicate radiocarbon ages analyzed on *N. pachyderma* (sin.).

[*Nydahl*, 1978], (3) measurement of nitrate concentration by chemiluminescence [*Braman and Hendrix*, 1989], and (4) bacterial conversion of nitrate to nitrous oxide [*Sigman et al.*, 2001], with measurement of the δ^{15}N of the nitrous oxide by gas chromatography-isotope ratio mass spectrometry [*Casciotti et al.*, 2002] using a Thermo MAT253 with a purpose-built nitrous oxide purge/trap/chromatography system at Princeton University.

Cleaning of foraminifera tests, following procedures described by *Straub et al.* [2013a], includes (1) 5 min ultrasonication in 2% sodium hexametaphosphate (pH 8), (2) reductive cleaning using sodium bicarbonate-buffered dithionite-citrate reagent, and (3) removal of external organic matter by persulfate oxidation.

The reproducibility of the δ^{15}N analyses of the nitrate resulting from individual organic N oxidations is consistently within 0.1‰. Replicates of the entire foraminifera cleaning-persulfate-denitrifier procedure were made when possible, and the standard deviation from this replication (generally smaller than 0.3‰) is indicated by vertical error bars in Figure 2b. FB-δ^{15}N results are reported in Table S1 in the supporting information.

Sediment purification and cleaning methods for diatom frustules (or opal fraction) are described by *Studer et al.* [2013]. Different size fractions of opal and hand-picked sponge spicules were analyzed and compared for δ^{15}N, in order to understand the isotopic contribution of nondiatom fraction (mostly from sponge spicules) and to understand the effect of diatom species difference. It was shown that contamination of N by nondiatomaceous opal should not normally compromise total DB-δ^{15}N (0–150 μm) because the nondiatom opal typically contributes

less than 5% to the total opal, except during the HS1 period [*Studer et al.*, 2013]. We also choose to use the 0–150 μm opal fraction as the total DB-δ^{15}N because this is the standard size fraction analyzed for DB-δ^{15}N in previous work. The particulars of the DB-δ^{15}N analyses are described by *Studer et al.* [2013].

2.3. Record of Eolian Dust Supply and Biogenic Fluxes

A history of eolian dust supply was reconstructed at this site using ^{230}Th-normalized ^{4}He flux at a depth resolution of 2–4 cm (Figure 2f). The measurement protocol and discussion of this record are provided by *Serno et al.* [2015].

[230]Th-normalized biogenic Ba flux, opal flux, and carbonate flux were measured at a resolution of 2–4 cm in order to reconstruct past changes in export production and its characteristics (Figures 2c, 2d, and 2e). The analyses were performed at LDEO, according to protocols described by *Serno et al.* [2014]. Complete results are presented in Serno et al. (in preparation). The average uncertainties are 2.3 mg/m^2/yr, 0.4 g/m^2/yr, and 0.1 g/m^2/yr, for biogenic Ba flux, opal flux, and carbonate flux, respectively.

3. Results

3.1. Nitrogen Isotopes

The δ^{15}N of all recorders is higher during the LGM. Unlike DB-δ^{15}N, FB-δ^{15}N does not decrease from the LGM into the HS1 time interval. FB-δ^{15}N varies little across LGM, HS1, and the early B/A; drops in the latter half of the B/A interval; rises briefly during the early YD; decreases sharply near the end of the YD; and then decreases gradually into the mid-Holocene (Figure 2).

The δ^{15}N variation through time is consistent between *G. bulloides* and *N. pachyderma*. *G. bulloides* is higher than *N. pachyderma* by ~3‰ throughout the record. This isotopic difference is also observed in the core-top sediments from the subarctic North Pacific (Ren, unpublished data) as well as in Holocene sediments from the sub-Antarctic [*Martínez-García et al.*, 2014].

After maintaining an offset of 2–3‰ from the LGM through the early B/A, *N. pachyderma* FB-δ^{15}N and DB-δ^{15}N begin to converge, finally reaching similar values at the end of the Preboreal period (at around 9 ka) and remaining similar throughout the remainder of the record. The isotopic difference is largest during the HS1 interval, when DB-δ^{15}N declines to values similar to those of the late Holocene.

3.2. Record of Eolian Dust Supply and Biogenic Fluxes

The ^{4}He$_{terr}$ flux record indicates high eolian dust supply to this region during the LGM and YD periods, in sharp contrast with the extremely low dust supply during the middle to late Holocene (Figure 2f) [*Serno et al.*, 2015]. The ^{230}Th-normalized biogenic fluxes at our study site were in general lowest during the last glacial period, slightly increased near the end of HS1, and reached a maximum during the B/A period. These fluxes are consistent with previous records from the NW Pacific (Figures 2c, 2d, and 2e). The fluxes of biogenic Ba and opal indicate qualitatively different histories since the LGM, with the biogenic opal flux of the later Holocene being similar to that of the LGM (Figures 2c and 2d). This observation will be addressed in a subsequent manuscript. Here we use the Ba data as the most general measure of export production, the rain of particulate organic matter exported from the euphotic zone (Figure 2d). Although barite can be mobilized when pore water sulfate is depleted by sulfate reduction [*Gingele et al.*, 1999], the absence of sulfidic conditions anytime during the past 150 kyr in sediments at nearby ODP Site 882 [*Jaccard et al.*, 2009] indicates that barite would have been well preserved. In this context, we interpret the compiled records to indicate that, relative to the Holocene, export production was lower during the LGM and that production may have been passed through a deglacial maximum during the B/A warm period. This interpretation follows those of *Keigwin et al.* [1992] and *Galbraith et al.* [2007].

4. Discussion

4.1. Glacial/Interglacial Changes in Nitrate Consumption in the Subarctic North Pacific

4.1.1. High Nitrate Consumption During the Last Glacial Maximum

While the quantitative differences among the FB- and DB-δ^{15}N records are of great interest, the fundamental finding of this study is that all fossil-bound recorders indicate higher δ^{15}N during the LGM than the Holocene. The observed high δ^{15}N suggests more complete nitrate consumption during the LGM. If shallow subsurface nitrate δ^{15}N were lower in the SNP during the LGM, a possible consequence of reduced denitrification in the NE Pacific, then this interpretation is simply reinforced [*Galbraith et al.*, 2008].

A large number of previous studies of the region, over multiple glacial cycles, indicate that export production was reduced during the ice ages in general and the LGM in particular [*Crusius et al.*, 2004; *Kienast et al.*, 2004; *Jaccard et al.*, 2005; *Brunelle et al.*, 2007, 2010; *Kohfeld and Chase*, 2011]. Thus, while perhaps counterintuitive, the degree of nitrate consumption was high when export production was low. The degree of nitrate consumption in the surface mixed layer is related to both the gross nitrate supply to the mixed layer and the uptake of nitrate, which leads to the eventual export of organic N:

$$\text{degree of nitrate consumption} = \text{uptake and export}/\text{supply}$$

According to this expression (or, more conveniently, supply = uptake/degree of nitrate consumption), a higher degree of consumption of the gross nitrate supply in the context of lower export production requires a decline in the gross supply rate of nitrate to the surface ocean. Thus, a change in the physical circulation must have reduced the import of the major nutrients into the euphotic zone during glacial times. Following previous work, we refer below to this reduced supply of deep water as stratification [*François et al.*, 1997; *Sigman et al.*, 2004], recognizing here that it may not speak directly to the density stratification of the glacial polar ocean (e.g., even with a constant density stratification, decreased wind-driven upwelling would decrease the nitrate supply). The data in hand cannot as yet distinguish which nitrate supply mechanism —upwelling or vertical mixing—decreased during ice ages, and a reduction in upwelling may in turn cause a reduction in vertical mixing [*Toggweiler et al.*, 2006; *de Boer et al.*, 2008].

A reduction in the gross nitrate supply to the SNP surface would not necessarily lead to more complete consumption of the available nitrate; nevertheless, it is the most likely outcome. Because marine phytoplankton productivity is at least partially limited by iron (Fe) [*Martin et al.*, 1990; *Boyd et al.*, 2004] and may be colimited by iron and light [*Sunda and Huntsman*, 1997; *Maldonado et al.*, 1999], an increase in the iron-to-nitrate (Fe/NO_3^-) supply ratio to the SNP surface ocean should cause nitrate consumption to rise. While both nitrate and Fe enter the surface mixed layer from subsurface waters, Fe is also supplied by Fe input from wind-supplied dust, lateral advection from the continental margins, continental Fe input from exposed shelves, Fe transport by icebergs, and the release of atmospherically derived Fe by summertime melting of sea ice [*Sedwick and DiTullio*, 1997]. We cannot address the Fe/NO_3^- ratio of subsurface water, but eolian Fe deposition was greater during the LGM (Figure 2f; *Serno et al.*, 2015), and the summertime margin of sea ice (with its winter's worth of deposited Fe) must have been closer to our site during ice ages. A reduction in nutrient supply from below would have rendered the eolian Fe input and other nondeep water Fe inputs proportionally more important, increasing the Fe/NO_3^- supply ratio and thus causing the degree of nitrate consumption to increase.

4.1.2. Different LGM-to-Holocene $\delta^{15}N$ Change Between Foraminifera and Diatoms

Depending on the sedimentary environment, there is the potential for diatom opal to be contaminated by the fragments of sponge spicules and radiolaria. In the SNP, the net effect of this contamination is to lower the measured DB-$\delta^{15}N$ [*Studer et al.*, 2013]. As a result, it is a logical hypothesis that the smaller $\delta^{15}N$ difference between the LGM and Holocene in diatom-bound N than in foraminifera-bound N is an artifact of contamination in the LGM opal. However, microscopic analyses of purified and cleaned diatoms from this site suggest only slightly greater radiolarian contamination in the LGM than in the Holocene and similar degrees of sponge spicule contamination, the latter being the greater concern because of its low $\delta^{15}N$ of ~−11‰ [*Studer et al.*, 2013]. Thus, we believe that the larger LGM-to-Holocene $\delta^{15}N$ change observed in foraminifera than in diatoms is a true upper ocean biogeochemical signal that warrants explanation. A possible explanation for the greater LGM elevation of FB-$\delta^{15}N$ relative to DB-$\delta^{15}N$ derives from the phenology of diatoms and foraminifera in the SNP, as described next.

The SNP is highly stratified throughout most of the year, with most nitrate supply occurring via wintertime deep mixing and subsequent uptake during spring and summer. In particular, in the northwestern North Pacific near our study site, where the winter mixing to the densest levels occurs today [*Ohno et al.*, 2009], almost all nitrate is supplied to the mixed layer during wintertime vertical mixing, while this deep mixing and the low incident sunlight cause nitrate assimilation rates to be low during this period. In the spring/summer period, the mixed layer shoals to ~20 m and the surface nitrate pool is consumed by phytoplankton, progressively raising the $\delta^{15}N$ of the residual nitrate, while resupply is weak, such that Rayleigh kinetics is an appropriate approximation of the system over the course of each productive spring-to-summer period. The concentration and $\delta^{15}N$ of mixed layer nitrate at the initiation of the summertime productivity peak can be estimated from the summertime subsurface temperature minimum ("dicothermal") layer (DL), which represents the base of the winter mixed layer that has been isolated from summertime production by the shoaling of the mixed layer into the summer. From hydrographic station K1 (51°N, 165°E), near the core site (Figure 1), modern DL nitrate concentration and $\delta^{15}N$ are 25.4 μM and 6.5‰, respectively (Figure 3).

The Rayleigh model, which assumes the consumption of a substrate in a closed system with constant isotopic fractionation, may be applied to quantify the $\delta^{15}N$ of the biomass produced in a given year during
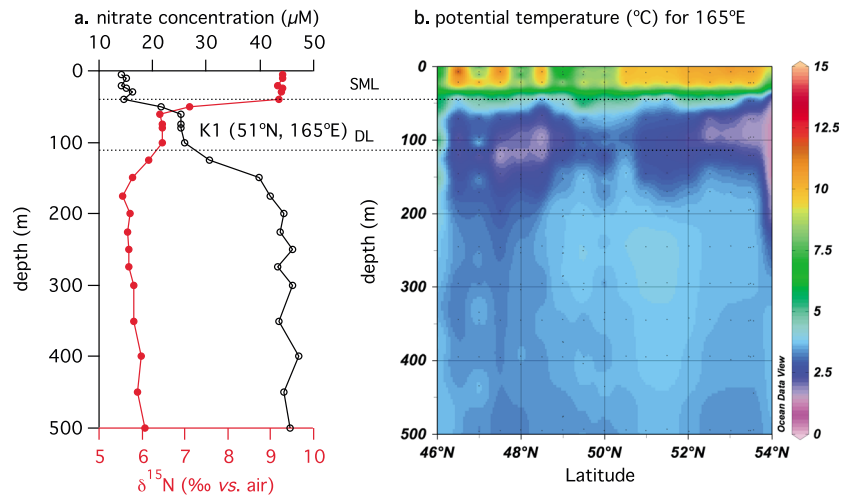
Figure 3. (a) The summer nitrate concentration (black circles) and nitrate δ^{15}N (red circles) profiles at station K1 (51°N, 165°E) close to our study site. These are reanalyses of the published data from this station [*Lehmann et al.*, 2005]. The profile indicates DL nitrate concentration and δ^{15}N are 25.4 μM and 6.5‰, respectively, and the summer-to-winter nitrate drawdown is ~10.5 μM, given the nitrate concentration in the summer mixed layer. (b) The potential temperature section for the WOCE transect P01 along 165°E between 46°N and 54°N for the upper 500 m water depth. The dashed lines indicate the base of the summer mixed layer (SML) and the core of the summertime subsurface temperature minimum ("dicothermal") layer (DL).

the spring-to-summer growth period (Figure 4, red and blue curves for the modern and LGM conditions, respectively):

$$\delta^{15}N_{nitrate} = \delta^{15}N_{initial\ nitrate\ source} - \varepsilon[\ln(f)] \tag{1}$$

$$\delta^{15}N_{instantaneous\ product} = \delta^{15}N_{initial\ nitrate\ source} - \varepsilon[1 + \ln(f)] \tag{2}$$

$$\delta^{15}N_{integrated\ product} = \delta^{15}N_{initial\ nitrate\ source} + \varepsilon[f/(1-f)]\ln(f) \tag{3}$$

Here f is the fraction of the remaining nitrate (i.e., summer nitrate concentration divided by winter nitrate concentration), ε is the isotope effect of nitrate assimilation, the instantaneous product is the organic N produced from nitrate assimilation at any given moment, and the integrated product is the organic N product accumulated over the event of progressive nitrate consumption (i.e., the instantaneous product integrated over the progressive decrease in f from 1 to its value at the end of the spring/summer growth period). While the δ^{15}N of the instantaneous product (Figure 4, dashed curve) closely tracks the increase in the δ^{15}N of nitrate, the δ^{15}N of the integrated product (Figure 4, solid curve) increases more weakly, with the greatest difference between the two at high degrees of nitrate consumption.

The total organic N exported from the surface mixed layer should be equivalent to the integrated product, as it integrates the organic matter produced over the spring-to-summer period of rapid growth and nitrate drawdown. However, the integrated product may apply less well to the organic matter produced by individual groups of organisms. Diatoms are among the first organisms to increase their growth into the spring/summer high-productivity period of the SNP, as indicated by silicate drawdown, sediment trap collections, and other observations [*Takahashi et al.*, 2000; *Kuroyanagi et al.*, 2002, 2008; *Asahi and Takahashi*, 2007]. The diatoms essentially drive the spring/summer nitrate drawdown, if anything becoming less important in the late summer and fall as coccolithophorids and other phytoplankton increase their importance. Thus, in the context of the Rayleigh model, the diatom biomass should approximate the integrated product in terms of changes in its δ^{15}N as a function of nitrate consumption, perhaps with a bias toward lower δ^{15}N than the integrated product.

In contrast to diatoms, the foraminifera acquire their N from the biomass of phytoplankton as well as higher trophic levels. As with other heterotrophs, they do not respond immediately to the springtime increase in phytoplankton growth in polar regions, increasing their number and biomass later in the spring/summer period. Indeed, observations from the SNP suggest that *N. pachyderma* and *G. bulloides* "bloom" in the summer to early fall, later than the spring diatom production increase [*Takahashi et al.*, 2000; *Asahi and Takahashi*, 2007].
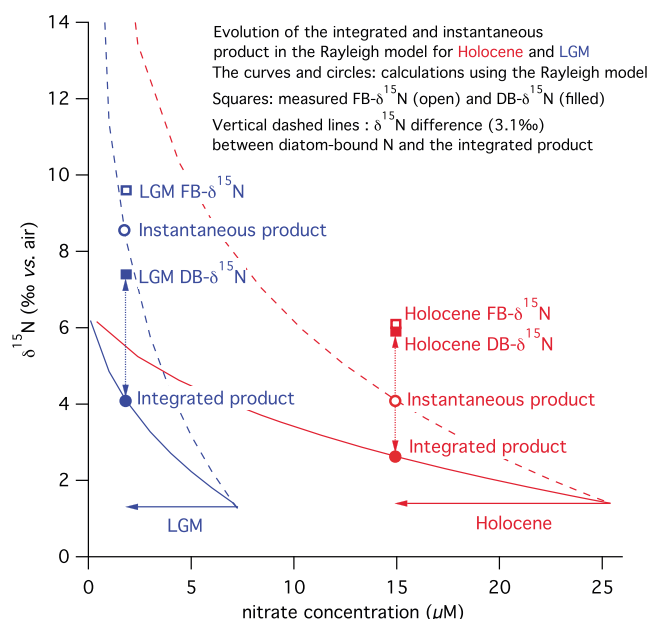
Figure 4. Evolution of the integrated and instantaneous product in the Rayleigh model based on our fossil $\delta^{15}N$ data and modern observations at western subarctic North Pacific water column station K1. The curves and circles represent calculations using the Rayleigh model. The measured averages, Holocene and LGM, for FB- and DB-$\delta^{15}N$ are shown in the open and filled squares (open = FB, filled = DB; Holocene = red, LGM = blue). Taking the wintertime nitrate concentration and $\delta^{15}N$ from K1, the modern summer time nitrate assimilation is assumed to follow the Rayleigh curve, such that the $\delta^{15}N$ of instantaneously produced N (red dashed line) increases exponentially with the degree of nitrate consumption, while the $\delta^{15}N$ of the integrated product (red solid line) increases more slowly. The summer nitrate drawdown (horizontal red arrow) of 10.5 μM yields an estimate of the $\delta^{15}N$ of the integrated product (red filled circle) and instantaneously produced N (red open circle). To simulate LGM nitrate assimilation (blue lines), we hold the DL nitrate $\delta^{15}N$ constant despite a lower DL nitrate concentration (see text). Based on biogenic barium fluxes, we assume that export production and thus spring-to-summer nitrate drawdown during the LGM (blue arrow) were 50% of the Holocene values. The DB-$\delta^{15}N$ measured for the Holocene and LGM (filled squares) suggests an increase in the $\delta^{15}N$ of the integrated product of ~1.5‰ during the LGM (from the red filled circle to the blue filled circle). This assumes that the difference between the measured core-top DB-$\delta^{15}N$ and the calculated $\delta^{15}N$ of the modern integrated product also applied to both the Holocene and the LGM (indicated by the vertical dashed lines). The Holocene difference between the measured DB-$\delta^{15}N$ and the calculated $\delta^{15}N$ of the modern integrated product is 3.1‰, which is likely due to the known offset between frustule $\delta^{15}N$ and biomass $\delta^{15}N$ (~2.6‰ [*Morales et al.*, 2014]). In order to simultaneously match the constraint on export production and the constraint on the degree of nitrate consumption from DB-$\delta^{15}N$, we calculate that winter and summer nitrate concentrations in the LGM were 7.3 and 2.0 μM, in comparison with 25.4 and 14.9 μM in the Holocene. Under the LGM condition of a greater degree of nitrate consumption, a greater $\delta^{15}N$ difference is expected between the instantaneous (blue open circle) and integrated product (blue filled circle). This can explain at least part of the greater $\delta^{15}N$ difference between FB- and DB-$\delta^{15}N$ during the last ice age. The core-top *N. pachyderma* FB-$\delta^{15}N$ is higher than the integrated product by 3.5‰, which is best interpreted as the trophic elevation of this heterotroph (~3‰ [*Persic et al.*, 2004]).

Their feeding thus may not allow them to record the diatom biomass produced at the initial stages of nitrate consumption. In contrast to the diatoms, FB-$\delta^{15}N$ should fall between the instantaneous and integrated products of the Rayleigh model.

At relatively low degrees of nitrate consumption, such as in the modern western SNP, the $\delta^{15}N$ difference between instantaneous and integrated products is modest (Figure 4: red open circle versus red filled circle). However, this difference increases dramatically with the degree of nitrate consumption. As *N. pachyderma* FB-$\delta^{15}N$ should behave as an intermediate between instantaneous and integrated products, FB-$\delta^{15}N$ should increase more with increasing nitrate consumption than the integrated product $\delta^{15}N$ and thus more than DB-$\delta^{15}N$. This distinction may thus explain the divergence between *N. pachyderma* FB-$\delta^{15}N$ and DB-$\delta^{15}N$ during the LGM (Figure 4).

A related possible contributor to the greater LGM elevation in FB-$\delta^{15}N$ than in DB-$\delta^{15}N$ involves the seasonal timing of nitrate drawdown. Given lower phytoplankton productivity during the LGM, nitrate consumption may have reached its end point earlier in the spring-to-summer progression (or not as much later as might be expected from the colder climate of the time). Thus, during the LGM, even with no change in the timing of the springtime increase in foraminifera relative to the initiation of the spring phytoplankton bloom, the bulk of the foraminifera production may have occurred when a greater proportion of the seasonal nitrate consumption had passed. In the terminology of the Rayleigh model, this would cause the LGM foraminifera to more completely approximate the instantaneous product, further raising FB-$\delta^{15}N$ relative to DB-$\delta^{15}N$.

These distinctions between diatom- and foraminifera-bound N as recorders of the degree of nitrate consumption in the SNP structure our discussion
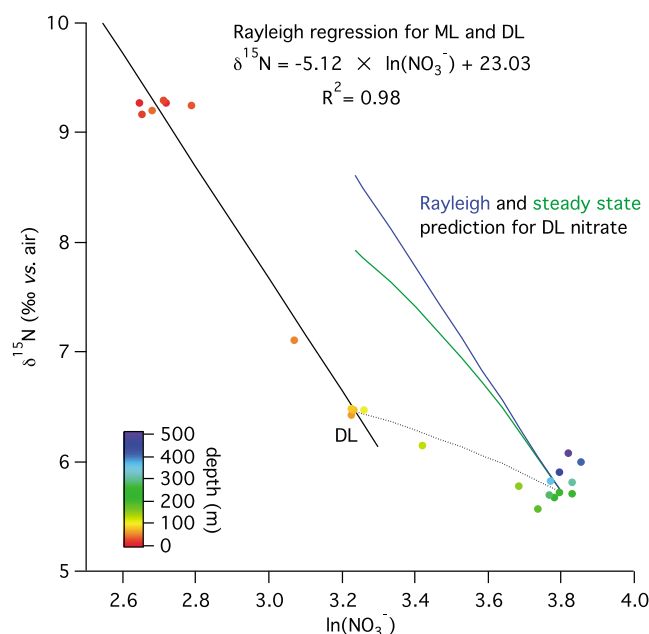
Figure 5. The summer mixed layer (ML) to DL nitrate concentration and $\delta^{15}N$ from station K1 (same data set from Figure 3a), when interpreted with the Rayleigh model (black solid line), suggest that the isotope effect for nitrate assimilation is ~5.1‰, as given by the slope of the regression. However, the $\delta^{15}N$ of the DL nitrate is much lower than the Rayleigh model (blue line) or steady state model (green line) predictions under the assumptions (1) that the thermocline nitrate between 200 and 300 m is the source for winter mixed layer and (2) there is a similar isotope effect of 5.1‰ during winter nitrate assimilation. The Rayleigh model assumes the consumption of a substrate in a closed system with constant isotopic fractionation, and the steady state model assumes that the net nitrate supply to the upper ocean (including the surface mixed layer and the underlying DL) is balanced by sinking organic N. The lower than predicted nitrate $\delta^{15}N$ of the DL may be the result of remineralization of low-$\delta^{15}N$ suspended PN within the DL (see text) [*Smart et al.*, 2015].

below. First, we use the DB-$\delta^{15}N$ data to reconstruct LGM-to-Holocene changes in the summertime decrease in SNP surface nitrate concentration. Second, we interpret the FB-$\delta^{15}N$ data of the two foraminifera species measured here, *N. pachyderma* (sin.) and *G. bulloides*, returning briefly to the question of what part of the seasonal nitrate drawdown is recorded by the foraminifera.

4.1.3. Calculation of Summertime Nitrate Consumption Using DB-$\delta^{15}N$

In order to quantify the degree of the spring/summer time nitrate consumption using the DB- or FB-$\delta^{15}N$ in the Rayleigh model, we must define the $\delta^{15}N$ of the nitrate supply at the beginning of the production season and choose a reasonable value for the isotope effect during nitrate assimilation. We do so by analyzing modern nitrate and $\delta^{15}N$ data from the western SNP region.

Much of the uncertainty in interpreting the diatom-bound N isotope data derives from the isotope dynamics of the winter mixed layer/dicothermal layer, which affects the nitrate $\delta^{15}N$/concentration relationship of the nitrate supplied to the spring/summer mixed layer (Figure 5). The upper ocean as a whole, which in the summer includes the surface mixed layer and the underlying DL while in the winter is simply the

mixed layer, can be considered as maintaining a long-term steady state with regard to N fluxes. Nitrate is in net imported into the upper ocean by diapycnal mixing across the base of the winter mixed layer (i.e., base of the DL), and this net nitrate supply is balanced by sinking organic N that passes across the base of the winter mixed layer before being remineralized. Given these conditions, the "steady state" model is expected to be more appropriate than the Rayleigh closed system model for the $\delta^{15}N$ of nitrate in the DL [*Hayes*, 2002; *Sigman et al.*, 1999, 2009]. In the steady state model, $\delta^{15}N$ of the nitrate (substrate) increases linearly with the degree of nitrate consumption, according to the isotope effect of nitrate assimilation:

$$\delta^{15}N_{reactant} = \delta^{15}N_{initial} + \varepsilon(1-f) \qquad (4)$$

where f is the fraction of reactant remaining. Thus, a lower rise in $\delta^{15}N$ for a given nitrate concentration decline in the DL is expected than if the Rayleigh model was applied (Figure 5 green line versus blue line).

In fact, nitrate in the modern DL has an even lower $\delta^{15}N$ than predicted by the steady state model (Figure 5, yellow points from around 100 m water depth). Studies of the Antarctic T_{min} layer (analogous to the DL of the SNP) suggest that this is largely due to the remineralization within the DL of low-$\delta^{15}N$ suspended particulate nitrogen (PN) remaining from the spring and summer periods [*Smart et al.*, 2015]. The net result is that the DL nitrate $\delta^{15}N$ (6.5‰) is only modestly higher than the nitrate $\delta^{15}N$ of underlying deep water (5.8‰) (yellow versus green points in Figure 5).

Despite the relatively low nitrate $\delta^{15}N$ of the DL in the modern SNP, one might imagine that DL nitrate $\delta^{15}N$ rose substantially during the LGM. The intuitive reason for this expectation is that more complete nitrate

consumption in the summer mixed layer would have produced very high δ^{15}N nitrate in the mixed layer, and this would have been mixed into the DL during the winter. However, under the higher degree of nitrate consumption of the LGM, as summertime nitrate consumption approaches completion, isotope fractionation during nitrate assimilation in the summer mixed layer is expressed in an increasingly small summer mixed layer nitrate pool. Consequently, when the summer mixed layer nitrate pool is mixed into the DL in the early winter, it raises the nitrate δ^{15}N of the DL only modestly, simply because the amount of residual nitrate in the mixed layer at the time of mixed layer deepening is so small. This dynamic, albeit in the very different oceanographic context of water column denitrification, was referred to as the "dilution effect" by *Deutsch et al.* [2004]. Because of the dilution effect, if nitrate consumption is nearly complete in the summer mixed layer, the δ^{15}N of nitrate in the winter mixed layer will not be significantly higher than that of underlying deep nitrate. Given this set of considerations, we make the simplifying assumption here that the DL nitrate δ^{15}N holds constant even as DL nitrate declines. Numerical modeling should be able to refine this approach in the future.

Using the data from station K1 and the Rayleigh model, an estimate can be generated for the δ^{15}N of modern N export in the SNP. The data from station K1 indicate a nitrate concentration and δ^{15}N of 25.4 μM and 6.5‰ in the DL (Figure 5, yellow points). Fitting of the Rayleigh model substrate equation (equation (1)) to the nitrate δ^{15}N and nitrate concentration data from the shallow DL and above at K1 yields an isotope effect for nitrate assimilation of 5.1‰ (Figure 5, solid black line). The modern summertime surface nitrate concentration is 14.9 μM. Accordingly, the δ^{15}N of the total exported N in the modern SNP is expected to be around 2.6‰. Core-top DB-δ^{15}N is measured to be ~5.9‰. A mean diatom biomass-to-frustule δ^{15}N difference of 2.6‰ has been measured in fresh net tow material collected in the Bering Sea [*Morales et al.*, 2014], such that the measured core-top DB-δ^{15}N should correspond to an exported diatom biomass δ^{15}N of 3.3‰. This is only 0.7‰ higher than the value predicted from station K1 and the Rayleigh model. Thus, given the known offset between frustule δ^{15}N and biomass δ^{15}N, the core-top DB-δ^{15}N is consistent with the calculated δ^{15}N of exported organic matter integrated over the spring/summer seasons.

DB-δ^{15}N is ~1.5‰ higher during the LGM than during the Holocene. Based on the reasoning in section 4.1.2 above, we infer that this δ^{15}N elevation applied to the accumulated spring-to-summer sinking N during the LGM. Given the biogenic barium fluxes (Figure 2d), one would infer that export production and thus spring-to-summer nitrate drawdown during the LGM were 50% of the Holocene values. In order to simultaneously match this constraint on export production and the constraint on the degree of nitrate consumption from DB-δ^{15}N, we calculate that winter and summer nitrate concentrations in the LGM were 7.1 and 1.8 μM, in comparison with 25.4 and 14.9 μM in the Holocene (Figure 4, blue curves). This calculation is different if the opal flux is taken as the measure of export production (Figure 2c). If we use opal flux to constrain changes on export production, the calculated winter and summer nitrate concentrations in the LGM would be 13.5 and 3.4 μM. Regardless of the details, a higher δ^{15}N in the context of lower or similar export production requires a significant decline in the gross supply rate of nitrate to the surface ocean during the LGM.

4.1.4. LGM-to-Holocene Changes in FB-δ^{15}N

The core-top *N. pachyderma* FB-δ^{15}N (6.1‰) is higher than the integrated product estimated from modern data by 3.5‰, similar to the findings in the subpolar North Atlantic [*Straub et al.*, 2013b]. This value is also similar to the offset between the estimated integrated product δ^{15}N and the measured DB-δ^{15}N of 3.3‰. In contrast to diatom frustules, the existing data on FB-δ^{15}N indicate no systematic elevation of the test-bound N relative to the organism's bulk biomass [*Ren et al.*, 2013]. The difference between measured *N. pachyderma* and calculated integrated product is indistinguishable from the elevation in δ^{15}N expected for one trophic level [*Persic et al.*, 2004]. Thus, the elevation of FB-δ^{15}N relative to the organic N produced over the summer by nitrate consumption is best interpreted as the trophic elevation of this heterotroph. Considering that *N. pachyderma* is a nonspinose and asymbiotic form that probably undertakes little predation [*Hemleben et al.*, 1989], a single level of trophic elevation appears reasonable. Subtracting a trophic ^{15}N enrichment of 3‰ [*Persic et al.*, 2004], the corrected core-top *N. pachyderma* FB-δ^{15}N (3.1‰) is similar to the integrated product δ^{15}N (2.6‰) in the modern condition. Above, we argue that, in this highly seasonal polar environment, FB-δ^{15}N may have a dependency on nitrate consumption that is intermediate between the integrated and instantaneous production equations of the Rayleigh model (equations (2) and (3)).

However, under the low degree of nitrate consumption in the modern SNP, the δ^{15}N of the integrated and instantaneous products is similar (Figure 4).

The FB-δ^{15}N of *G. bulloides* and *N. pachyderma* appear to maintain a roughly constant difference (~3‰) throughout the record. This difference is consistent with core-top measurements from different regions (A. Martínez-García, personal communications, 2013). It is most likely that the δ^{15}N difference reflects a dietary difference, as both species are asymbiotic. It is unclear, however, whether the dietary δ^{15}N difference originates from differences in trophic level or in depth/seasonal habitats. Our current knowledge regarding their ecological difference in the polar ocean is insufficient to address such questions. Nevertheless, the constant δ^{15}N difference between the two species suggests that the ecological factors driving the difference likely remained unchanged from LGM to the Holocene, providing an additional reason for confidence that the δ^{15}N change recorded in both species is driven by a broad environmental change, specifically, a change in the degree of nitrate consumption.

As outlined above, we argue that the greater LGM FB-to-DB δ^{15}N difference results fundamentally from the tendency of FB-δ^{15}N, in this highly seasonal environment of the western SNP, to lag the autotrophic spring bloom, causing them to preferentially capture late spring-to-summer nitrate conditions. Two possible specific mechanisms for the greater FB-to-DB δ^{15}N difference during the LGM are (1) a greater δ^{15}N difference between instantaneous and integrated products as the fractional nitrate consumption increases (Figure 4) and (2) a higher degree of nitrate consumption by the time of most foraminifera growth during the LGM, which is arguably to be expected when a given amount of nitrate drawdown represents a greater degree of nitrate consumption. Considering the first effect in isolation, the reconstructed LGM nitrate drawdown would have caused the instantaneous product/integrated product δ^{15}N difference to rise by ~2.5‰ (Figure 4), indistinguishable from the ~2.0‰ rise in the DB-δ^{15}N/FB-δ^{15}N difference during the LGM. However, this effect alone is unlikely to explain the entire change in the DB-δ^{15}N/FB-δ^{15}N difference, as FB-δ^{15}N probably has a behavior that is intermediate between the instantaneous and integrated products. Thus, the second effect was probably also significant.

Here, we take a step toward quantifying the relative importance of these two dynamics with a calculation based on the Rayleigh model. In this calculation, the instantaneous product is integrated across different ranges of *f* for diatoms and foraminifera. Accordingly, the δ^{15}N difference between FB- and DB-δ^{15}N is set by (1) the fraction of nitrate remaining at the beginning of foraminifera production (f_a) and (2) the fraction of nitrate remaining by the end of the summer growth period (f_b) (Figure 6). This δ^{15}N difference has the following expression in terms of f_a and f_b:

$$\text{FB-}\delta^{15}\text{N} - \text{DB-}\delta^{15}\text{N} = \varepsilon \left[(f_a - f_b)(1 - f_b)\right]^{-1} \ln\left[f_a^{(1-f_a)} f_b^{-(1-f_b)}\right] \tag{5}$$

where ε is the isotope effect of nitrate assimilation.

To make use of this expression, we must relate FB- and DB-δ^{15}N to the autotrophic biomass being produced in the surface ocean at any given time. For this purpose, both Holocene and LGM mean δ^{15}N have been offset downward, by 2.6‰ for DB-δ^{15}N and of 3‰ for FB-δ^{15}N of *N. pachyderma*. The DB-δ^{15}N offset is interpreted here as a diatom frustule-to-biomass δ^{15}N difference and is consistent with known offsets from field data [*Morales et al.*, 2014]. As described above, the *N. pachyderma* FB-δ^{15}N offset is interpreted here as a trophic-level enrichment effect of 3‰ for FB-δ^{15}N of *N. pachyderma*. The LGM DB-δ^{15}N increase defines the decrease of f_b during the LGM, which indicates that greater than 80% of the nitrate supply was consumed during the LGM. From the Holocene and LGM values for the difference between FB-δ^{15}N and DB-δ^{15}N, f_a is then calculated for both Holocene and LGM. It is calculated that f_a was ~40% lower during the LGM than during the Holocene, or roughly ~52% during the LGM. The inference is that, during the LGM, about half of the seasonal nitrate consumption had occurred before foraminifera production rose to substantial levels. Of course, there are multiple sources of uncertainty in this calculation, not the least of which is the applicability of the Rayleigh model. Nevertheless, this interpretation may be testable with other paleoceanographic proxy data and/or through studies of foraminiferal seasonality in the modern ocean.

4.2. Deglacial Changes in Nitrate Consumption in the Subarctic Pacific
4.2.1. High Nitrate Consumption During the Early Deglacial (HS1)
The HS1 DB-δ^{15}N decline observed in this and other sediment cores across the North Pacific [*Brunelle et al.*, 2007, 2010; *Studer et al.*, 2013] is not observed in FB-δ^{15}N (Figure 2b). The HS1 interval sediments have the
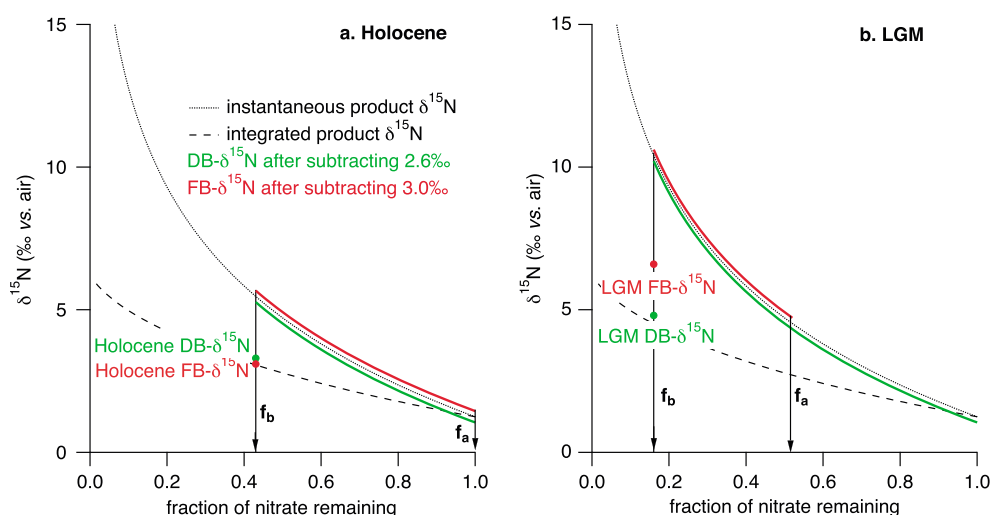
Figure 6. Interpretation of the LGM-to-Holocene change in the δ^{15}N difference of planktonic foraminifera and diatoms based on the Rayleigh model, with the (a) Holocene and (b) LGM cases shown. f_a is the fraction of nitrate remaining at the beginning of foraminifera production, and f_b is the fraction of nitrate remaining by the end of the summer growth period. Diatoms are among the first organisms to increase their growth into the spring/summer high-productivity period of the SNP and essentially drive the spring/summer nitrate drawdown. Thus, it is assumed that DB-δ^{15}N (in green) approximates the integrated product, in that diatom production is associated with the entire progress of nitrate consumption, from no nitrate consumption to an end-of-season degree of nitrate consumption. In contrast, planktonic foraminifera may not closely track the early phytoplankton growth in the spring, causing FB-δ^{15}N (in red) to fall between the instantaneous and integrated products in the Rayleigh model. FB-δ^{15}N is assumed to integrate over only a portion of the nitrate consumption, starting at f_a and ending at f_b. f_b is calculated using the DB-δ^{15}N data alone, and f_a is then calculated from the FB-δ^{15}N data. FB- and DB-δ^{15}N have been related to the autotrophic biomass being produced in the surface ocean by offsetting DB-δ^{15}N downward by 2.6‰ and FB-δ^{15}N of *N. pachyderma* downward by 3.0‰ (see text). The slight mismatch between calculated diatom biomass δ^{15}N and the integrated product δ^{15}N is due to the fact that f_b in Figure 6a is calculated based on the water column data in Figures 3 and 5 and not the mean DB-δ^{15}N. In Figure 6b, f_b is calculated from DB-δ^{15}N, assuming that the Holocene δ^{15}N difference between calculated diatom biomass and integrated product δ^{15}N also applies in the LGM.

lowest opal content of the last glacial cycle [*Brunelle et al.*, 2007] and a distinctive texture. Microscopic investigation of the opal analyzed in HS1 sediments revealed significant contamination by nondiatom opal, both sponge spicules and radiolaria [*Studer et al.*, 2013]. Given the quantified spicule content in the purified opal, its low δ^{15}N (~ −11‰) can entirely explain the HS1 DB-δ^{15}N decline, absent any changes in nitrate consumption [*Studer et al.*, 2013].

Being analyzed on handpicked specimens, FB-δ^{15}N has the advantage of not being contaminated with nonforaminiferal material. In contrast to DB-δ^{15}N, the constant FB-δ^{15}N across the HS1 interval presented here unambiguously indicates that nitrate consumption in the SNP remained high and constant from the LGM across the early deglacial HS1 period. These data thus support the suggestion of *Studer et al.* [2013] that the HS1 DB-δ^{15}N decline is an artifact of nondiatom opal contamination.

This finding greatly simplifies interpretation of a single relationship between regional climate and nitrate supply from below across the HS1 in the subarctic North Pacific. It has been a conceptual challenge to explain why nutrient consumption would undergo a sharp decrease at HS1, a time when there is no evidence for a clear change in productivity [*Crusius et al.*, 2004; *Brunelle et al.*, 2007, 2010; *Jaccard et al.*, 2009; *Kohfeld and Chase*, 2011]. The hypothesis of *Brunelle et al.* [2010] and *Lam et al.* [2013] for these coupled observations was that the HS1 brought a deeper mixed layer and thus light limitation of SNP phytoplankton. Given our new understanding of the N isotope data, the HS1 is best interpreted as a continuation of ice age stratification in the SNP. Our data cannot rule out the possibility that intermediate water may have been ventilated from a geographically small local source, such as the Sea of Okhotsk; however, it argues against widespread vertical mixing throughout the western subarctic North Pacific during the LGM and HS1.

4.2.2. Changes in Nitrate Consumption in the Late Deglacial (B/A-YD) and Holocene

For both *N. pachyderma* and *G. bulloides*, FB-δ^{15}N does not undergo a clear change at the transition from HS1 into the B/A interval (Figure 2). This is in stark contrast to bulk sediment and DB-δ^{15}N data from this and other

cores [*Brunelle et al.*, 2010], which show a sharp δ^{15}N increase into the B/A. Along the lines of the discussion above, an artificially low δ^{15}N in HS1 due to sponge spicule contamination can explain the subsequent δ^{15}N rise in bulk sediment and diatom-bound N, as sedimentary opal and biogenic sediment as a whole rose sharply at the B/A, causing sponge spicule contamination to become minor [*Studer et al.*, 2013].

At face value, the FB-δ^{15}N data imply similar values for assimilated nitrate during the early B/A as during HS1 and the LGM, with δ^{15}N declining in the middle or late B/A. Pairing a similar or lower degree of nitrate consumption during the B/A with much higher biogenic fluxes to the seafloor at the B/A implies a sharp increase in the rate of nitrate supply to the surface ocean at the HS1-to-B/A transition. Furthermore, eastern North Pacific sediment records appear to record deglacial maxima in subsurface nitrate δ^{15}N, during the B/A in particular [*Ganeshram et al.*, 1995; *Pride et al.*, 1999; *Chang et al.*, 2008; *Galbraith et al.*, 2008; *Addison et al.*, 2012]. If this change applied to the western SNP, then it may have overprinted and thus hidden a nitrate consumption-driven FB-δ^{15}N decline across the transition from HS1 to B/A. If there was a decline in the degree of nitrate consumption at the HS1-to-B/A transition, then, in combination with the pronounced increase in export production at the B/A (Figures 2c and 2d), the implied HS1-to-B/A rise in nitrate supply to the euphotic zone was even greater. These uncertainties aside, the data argue that SNP surface/subsurface exchange increased dramatically at the onset of the B/A and not during HS1 as previously suggested [*Gebhardt et al.*, 2008; *Brunelle et al.*, 2010; *Okazaki et al.*, 2010; *Lam et al.*, 2013; *Rae et al.*, 2014].

Reciprocally, FB-δ^{15}N suggests a transient rise in δ^{15}N within the early YD interval (Figure 2b). Based on data from this and many other SNP cores, the YD is reconstructed as a time of lower productivity (Figure 2). Coupled with the coincident rise in FB-δ^{15}N, the data suggest a decline in nitrate supply at this time, consistent with the general pattern of greater stratification in the SNP during periods of colder climate in the Northern Hemisphere.

In summary, the FB-δ^{15}N records, in the context of the biogenic flux data, make a strong case for a single relationship between regional climate and gross nitrate supply from below, with reduced nitrate supply (i.e., stratification) under regionally cold climate.

5. Conclusions and Perspective

The modern SNP is strongly stratified by a buoyant, low-salinity surface layer, which is sustained by an excess in precipitation and runoff relative to evaporation and restricted meridional exchange between subpolar and subtropical surface waters [*Warren*, 1983; *Emile-Geay et al.*, 2003]. Reconstructions of changes in surface salinity and temperature have led some authors to hypothesize dramatic departures from this halocline-dominated condition during intervals within the deglaciation [*Keigwin et al.*, 1992; *Sarnthein et al.*, 2004, 2006; *Okazaki et al.*, 2010; *Gebhardt et al.*, 2008; *Sagawa and Ikehara*, 2008]. In particular, it has been suggested that there was direct ventilation of the deep ocean from the North Pacific surface during HS1, potentially contributing to the first pulse of deglacial atmospheric CO_2 rise [*Okazaki et al.*, 2010; *Rae et al.*, 2014]. This argument appears to be consistent with some reconstructions of the radiocarbon and oxygen contents of the North Pacific [*Crusius et al.*, 2004; *Okazaki et al.*, 2010; *Menviel et al.*, 2012; *Rae et al.*, 2014] and can be argued to fit with existing DB-δ^{15}N records from the open SNP and Bering Sea [*Brunelle et al.*, 2007, 2010]. Mechanisms proposed for driving the HS1 deep convection in the SNP focus on linkages between the North Atlantic and North Pacific. For example, some modeling results show inverse overturning behavior between the North Pacific and North Atlantic across the deglaciation, through feedbacks between salinity anomalies and ocean circulation [*Saenko et al.*, 2004; *Schmittner et al.*, 2007; *Okazaki et al.*, 2010].

However, other observations regarding the deglacial events in the SNP challenge this interpretation. The compiled records do not show a clear sign of enhanced ventilation during HS1 below 1300 m water depth, suggesting that local ventilation, if it occurred during HS1, was restricted to shallow depths [*Jaccard and Galbraith*, 2013]. Further, other stable isotope and radiocarbon data suggest a significant increase in deep ocean ventilation in the North Pacific at the onset of the B/A (e.g., Figure 2a), but not prior to it [*Keigwin*, 1998; *Galbraith et al.*, 2007].

Almost all existing productivity records from the SNP show no or only a modest increase during HS1 (Figure 2) [*Crusius et al.*, 2004; *Brunelle et al.*, 2007, 2010; *Jaccard et al.*, 2009; *Kohfeld and Chase*, 2011]. In contrast, a large and coherent peak in biogenic fluxes in the open subarctic North Pacific occurred during the B/A. Various scenarios have been considered for this sequence of changes, with arguments that the

increased productivity at the B/A was a response to greater nutrient supply associated with increased wind-driven upwelling, greater vertical mixing, or a rise in shallow subsurface nutrient concentrations [*Galbraith et al.*, 2007; *Gebhardt et al.*, 2008; *Davies et al.*, 2011; *Addison et al.*, 2012]. In contrast, *Lam et al.* [2013] explained the low productivity during HS1 in the SNP by light limitation on productivity due to deep mixing and interpreted the B/A productivity peak as a response to the subsequent shutdown in this mixing. This last interpretation and related interpretations that involve deep water formation during HS1 would require a breakdown in the coupling between cold climate and reduced vertical exchange that appears to characterize the glacial state [*Jaccard et al.*, 2005; *Brunelle et al.*, 2007, 2010; *Galbraith et al.*, 2008].

As described above, the deglacial changes in FB-δ^{15}N reconstructed here are inversely correlated with changes in biogenic flux. Taking these data together, it is implied that deglacial and interglacial periods of high export production are associated with greater nitrate supply from below and do not simply reflect a rise in the degree to which a given nitrate supply was consumed. During HS1, the SNP maintained the glacial conditions of low nutrient supply from below, that is, stratification. This condition does not appear to have changed until the B/A interval, which was associated with warming in the Northern Hemisphere, including the North Pacific [*Kiefer and Kienast*, 2005; *Max et al.*, 2012; *Praetorius and Mix*, 2014]. In contrast to *Lam et al.* [2013], based on the combination of decreased FB-δ^{15}N and increased biogenic fluxes, we conclude that the B/A was a time of dramatically increased gross nitrate supply to the SNP surface waters. The near-diametric opposition of our interpretation of HS1 and B/A conditions to that of *Lam et al.* [2013], with LGM-like stratification during HS1 and active vertical supply of nutrients during the B/A, originates from the FB-δ^{15}N data and their confirmation that the DB-δ^{15}N decline during the HS1 was an artifact of sponge spicule contamination. The brief increase in FB-δ^{15}N and the decline in biogenic fluxes during the colder YD can be explained by a return to stratified conditions. In summary, our FB-δ^{15}N data are consistent with the view that the glacial/interglacial association of Northern Hemisphere cold climate with SNP stratification and of warm climate with greater surface-to-deep exchange applied to the deglacial events as well.

References

Addison, J. A., B. P. Finney, W. E. Dean, M. H. Davies, A. C. Mix, J. S. Stoner, and J. M. Jaeger (2012), Productivity and sedimentary δ^{15}N variability for the last 17,000 years along the northern Gulf of Alaska continental slope, *Paleoceanography*, 27, PA1206, doi:10.1029/2011PA002161.

Anderson, R. F., S. Ali, L. I. Bradtmiller, S. H. H. Nielsen, M. Q. Fleisher, B. E. Anderson, and L. H. Burckle (2009), Wind-driven upwelling in the Southern Ocean and the deglacial rise in atmospheric CO_2, *Science*, 323, 1443–1448.

Asahi, H., and K. Takahashi (2007), A 9-year time-series of planktonic foraminifer fluxes and environmental change in the Bering sea and the central subarctic Pacific Ocean, 1990–1999, *Prog. Oceanogr.*, 72, 343–363.

Boyd, P. W., et al. (2004), The decline and fate of an iron-induced subarctic phytoplankton bloom, *Nature*, 428, 549–553.

Braman, R. S., and S. A. Hendrix (1989), Nanogram nitrite and nitrate determination in environmental and biological materials by V(III) reduction with chemiluminescence detection, *Anal. Chem.*, 61, 2715–2718.

Brunelle, B. G., D. M. Sigman, M. S. Cook, L. D. Keigwin, G. H. Haug, B. Plessen, G. Schettler, and S. L. Jaccard (2007), Evidence from diatom bound nitrogen isotopes for subarctic Pacific stratification during the last ice age and a link to North Pacific denitrification changes, *Paleoceanography*, 22, PA1215, doi:10.1029/2005PA001205.

Brunelle, B. G., D. M. Sigman, S. L. Jaccard, L. D. Keigwin, B. Plessen, G. Schettler, M. S. Cook, and G. H. Haug (2010), Glacial/interglacial changes in nutrient supply and stratification in the western subarctic North Pacific since the penultimate glacial maximum, *Quat. Sci. Rev.*, 29, 2579–2590, doi:10.1016/j.quascirev.2010.03.010.

Cannariato, K., and J. Kennett (1999), Climatically related millennial-scale fluctuations in strength of California margin oxygen-minimum zone during the past 60 k.y, *Geology*, 27, 975–978.

Casciotti, K. L., D. M. Sigman, M. G. Hastings, J. K. Bohlke, and A. Hilkert (2002), Measurement of the oxygen isotopic composition of nitrate in seawater and freshwater using the denitrifier method, *Anal. Chem.*, 74(19), 4905–4912.

Chang, A. S., T. F. Pedersen, and I. L. Hendy (2008), Late Quaternary paleoproductivity history on the Vancouver Island margin, western Canada: a multiproxy geochemical study, *Can. J. Earth Sci.*, 45, 1283–1297.

Cook, M. S., L. D. Keigwin, and C. A. Sancetta (2005), The deglacial history of surface and intermediate water of the Bering Sea, *Deep Sea Res., Part II*, 52, 2163–2173.

Crusius, J., T. F. Pedersen, S. Kienast, L. Keigwin, and L. Labeyrie (2004), Influence of northwest Pacific productivity on North Pacific Intermediate Water oxygen concentrations during the Bolling-Allerod interval (14.7–12.9 ka), *Geology*, 32(7), 633–636.

Davies, M. H., A. C. Mix, J. S. Stoner, J. A. Addison, J. Jaeger, B. Finney, and J. Wiest (2011), The deglacial transition on the southeastern Alaska Margin: Meltwater input, sea level rise, marine productivity, and sedimentary anoxia, *Paleoceanography*, 26, PA2223, doi:10.1029/2010PA002051.

de Boer, A. M., D. M. Sigman, and J. R. Toggweiler (2008), The effect of global ocean temperature change on deep ocean ventilation, *Paleoceanography*, 22, PA2210, doi:10.1029/2005PA001242.

Deutsch, C., D. M. Sigman, R. C. Thunell, A. N. Meckler, and G. H. Haug (2004), Isotopic constraints on glacial/interglacial changes in the oceanic nitrogen budget, *Global Biogeochem. Cycles*, 19, GB4012, doi:10.1029/2003GB002189.

Emile-Geay, J., M. A. Cane, N. Naik, R. Seager, A. C. Clement, and A. van Geen (2003), Warren revisited: Atmospheric freshwater fluxes and "why is no deep water formed in the North Pacific", *J. Geophys. Res.*, 108(C6), 3178, doi:10.1029/2001JC001058.

François, R., M. A. Altabet, E.-F. Yu, D. M. Sigman, M. P. Bacon, M. Frank, G. Bohrmann, G. Bareille, and L. D. Labeyrie (1997), Contributions of Southern Ocean surface-water stratification to low atmospheric CO_2 concentrations during the last glacial period, *Nature*, *389*(6654), 929–935.

Galbraith, E. D., S. L. Jaccard, T. F. Pedersen, D. M. Sigman, G. H. Haug, M. Cook, J. R. Southon, and R. François (2007), Carbon dioxide release from the North Pacific abyss during the last deglaciation, *Nature*, *449*, 890–893.

Galbraith, E. D., M. Kienast, S. L. Jaccard, T. F. Pedersen, B. G. Brunelle, D. M. Sigman, and T. Kiefer (2008), Consistent relationship between global climate and surface nitrate utilization in the western subarctic Pacific throughout the last 500 ka, *Paleoceanography*, *23*, PA2212, doi:10.1029/2007PA001518.

Ganeshram, R. S., T. F. Pedersen, S. E. Calvert, and J. W. Murray (1995), Large changes in ocean nutrient inventories from glacial to interglacial periods, *Nature*, *376*(6543), 755–758.

García, H. E., R. A. Locarnini, T. P. Boyer, J. I. Antonov, M. M. Zweng, O. K. Baranova, and D. R. Johnson (2010), in *World Ocean Atlas 2009, Volume 4: Nutrients (Phosphate, Nitrate, Silicate)*, *NOAA Atlas NESDIS*, vol. 71, edited by S. Levitus, 398 pp., U.S. Gov. Print. Off., Washington, D. C.

Gebhardt, H., M. Sarnthein, P. M. Grootes, T. Kiefer, H. Kuehn, F. Schmieder, and U. Röhl (2008), Paleonutrient and productivity records from the subarctic North Pacific for Pleistocene glacial terminations I to V, *Paleoceanography*, *23*, PA4212, doi:10.1029/2007PA001513.

Gersonde, R. (2012), The expedition of the research vessel "Sonne" to the subpolar North Pacific and the Bering Sea in 2009 (SO202-INOPEX), *Rep. Polar Mar. Res.*, *643*, 1–323.

Gingele, F. X., M. Zabel, S. Kasten, W. J. Bonn, and C. C. Nürnberg (1999), Biogenic barium as a proxy for paleoproductivity: Methods and limits of application, in *Use of Proxies in Paleoceanography: Examples From the South Atlantic*, edited by G. Fischer and G. Wefer, pp. 345–364, Springer, Berlin.

Hain, M. P., D. M. Sigman, and G. H. Haug (2010), Carbon dioxide effects of Antarctic stratification, North Atlantic Intermediate Water formation, and subantarctic nutrient drawdown during the last ice age: Diagnosis and synthesis in a geochemical box model, *Global Biogeochem. Cycles*, *24*, GB4023, doi:10.1029/2010GB003790.

Haug, G. H., D. M. Sigman, R. Tiedemann, T. F. Pedersen, and M. Sarnthein (1999), Onset of permanent stratification in the subarctic Pacific Ocean, *Nature*, *401*, 779–782.

Hayes, J. (2002), *Practice and Principles of Isotopic Measurements in Organic Geochemistry (Revision 2)*, pp. 1–25, Woods Hole Oceanographic Institution, Woods Hole, Mass.

Hemleben, C., M. Spindler, and O. R. Anderson (1989), *Modern Planktonic Foraminifera*, pp. 1–363, Springer, New York.

Jaccard, S. L., and E. D. Galbraith (2013), Direct ventilation of the North Pacific did not reach the deep ocean during the last deglaciation, *Geophys. Res. Lett.*, *40*, 199–203, doi:10.1029/2012GL054118.

Jaccard, S. L., G. H. Haug, D. M. Sigman, T. F. Pedersen, H. R. Thierstein, and U. Rohl (2005), Glacial/interglacial changes in subarctic North Pacific stratification, *Science*, *308*(5724), 1003–1006.

Jaccard, S. L., E. D. Galbraith, D. M. Sigman, G. H. Haug, R. François, T. F. Pedersen, P. Dulski, and H. R. Thierstein (2009), Subarctic Pacific evidence for a glacial deepening of the oceanic respired carbon pool, *Earth Planet. Sci. Lett.*, *277*, 156–165.

Keigwin, L., G. A. Jones, and P. N. Froelich (1992), A 15,000 year paleoenvironmental record from Meiji Seamount, far northwestern Pacific, *Earth Planet. Sci. Lett.*, *111*, 425–440.

Keigwin, L. D. (1998), Glacial-age hydrography of the far northwest Pacific Ocean, *Paleoceanography*, *13*(4), 323–339.

Kiefer, T., and M. Kienast (2005), Patterns of deglacial warming in the Pacific Ocean: A review with emphasis on the time interval of Heinrich event 1, *Quat. Sci. Rev.*, *24*, 1063–1081.

Kienast, S. S., I. L. Hendy, J. Crusius, T. F. Pedersen, and S. E. Calvert (2004), Export production in the subarctic North Pacific over the last 800 kyrs: No evidence for iron fertilization?, *J. Oceanogr.*, *60*(1), 189–203.

Knapp, A. N., D. M. Sigman, and F. Lipschultz (2005), N isotopic composition of dissolved organic nitrogen and nitrate at the Bermuda Atlantic time-series study site, *Global Biogeochem. Cycles*, *19*, GB1018, doi:10.1029/2004GB002320.

Kohfeld, K. E., and Z. Chase (2011), Controls on deglacial changes in biogenic fluxes in the North Pacific Ocean, *Quat. Sci. Rev.*, *30*, 3350–3363.

Kuroyanagi, A., H. Kawahata, H. Nishi, and C. M. Honda (2002), Seasonal changes in planktonic foraminifera in the northwestern North Pacific Ocean: Sediment trap experiments from subarctic and subtropical gyres, *Deep Sea Res., Part II*, *49*, 5627–5645.

Kuroyanagi, A., H. Kawahata, H. Nishi, and M. C. Honda (2008), Seasonal to interannual changes in planktonic foraminiferal assemblages in the northwestern North Pacific: Sediment trap results encompassing a warm period related to El Niño, *Palaeogeogr. Palaeoclimatol. Palaeoecol.*, *262*, 107–127.

Lam, P. J., L. F. Robinson, J. Blusztajn, C. Li, M. S. Cook, J. F. McManus, and L. D. Keigwin (2013), Transient stratification as the cause of the North Pacific productivity spike during deglaciation, *Nat. Geosci.*, *6*, 622–626, doi:10.1038/NGEO1893.

Lehmann, M. F., D. M. Sigman, D. C. McCorkle, B. G. Brunelle, S. Hoffmann, M. Kienast, G. Cane, and J. Clement (2005), Origin of the deep Bering Sea nitrate deficit: Constraints from the nitrogen and oxygen isotopic composition of water column nitrate and benthic nitrate fluxes, *Global Biogeochem. Cycles*, *19*, GB4005, doi:10.1029/2005GB002508.

Maldonado, M. T., P. W. Boyd, P. J. Harrison, and N. M. Price (1999), Co-limitation of phytoplankton growth by light and Fe during winter in the NE subarctic Pacific Ocean, *Deep Sea Res., Part II*, *46*, 2475–2485.

Martin, J. H., S. E. Fitzwater, and R. M. Gordon (1990), Iron deficiency limits growth in Antarctic waters, *Global Biogeochem. Cycles*, *4*, 5–12, doi:10.1029/GB004i001p00005.

Martínez-García, A., D. M. Sigman, H. Ren, R. F. Anderson, M. Straub, D. A. Hodell, S. L. Jaccard, T. I. Eglinton, and G. H. Haug (2014), Iron fertilization of the Subantarctic Ocean during the Last Ice Age, *Science*, *343*, 1347–1350.

Max, L., J.-R. Riethdorf, R. Tiedemann, M. Smirnova, L. Lembke-Jene, K. Fahl, D. Nürnberg, A. Matul, and G. Mollenhauer (2012), Sea surface temperature variability and sea-ice extent in the subarctic northwest Pacific during the past 15,000 years, *Paleoceanography*, *27*, PA3213, doi:10.1029/2012PA002292.

Meckler, A. N., H. Ren, D. M. Sigman, N. Gruber, B. Plessen, C. J. Schubert, and G. H. Haug (2011), Deglacial nitrogen isotope changes in the Gulf of Mexico: Evidence from bulk sedimentary and foraminifera-bound nitrogen in Orca Basin sediments, *Paleoceanography*, *26*, PA4216, doi:10.1029/2011PA002156.

Menviel, L., A. Timmermann, O. Elison Timm, A. Mouchet, A. Abe-Ouchi, M. O. Chikamoto, N. Harada, R. Ohgaito, and Y. Okazaki (2012), Removing the North Pacific halocline: Effects on global climate, ocean circulation and the carbon cycle, *Deep Sea Res., Part II*, *61–64*, 106–113, doi:10.1016/j.dsr2.2011.03.005.

Morales, L. V., J. Granger, B. X. Chang, M. G. Prokopenko, B. Plessen, R. Gradinger, and D. M. Sigman (2014), Elevated $^{15}N/^{14}N$ in particulate organic matter, zooplankton, and diatom frustule-bound nitrogen in the ice-covered water column of the Bering sea eastern shelf, *Deep Sea Res., Part II*, *109*, 100–111, doi:10.1016/j.dsr2.2014.05.008.

North Greenland Ice Core Project members (2004), High-resolution record of Northern Hemisphere climate extending into the last interglacial period, *Nature*, *431*(7005), 147–151.

Nydahl, F. (1978), Peroxodisulfate oxidation of total nitrogen in waters to nitrate, *Water Res.*, *12*, 1123–1130.

Ohno, Y., N. Iwasaka, F. Kobashi, and Y. Sato (2009), Mixed layer depth climatology of the North Pacific based on Argo observations, *J. Oceanogr.*, *65*, 1–16.

Okazaki, Y., A. Timmermann, L. Menviel, N. Harada, A. Abe-Ouchi, M. O. Chikamoto, A. Mouchet, and H. Asahi (2010), Deepwater formation in the North Pacific during the last glacial termination, *Science*, *329*, 200–204, doi:10.1126/science.1190612.

Persic, A., H. Roche, and F. Ramada (2004), Stable carbon and nitrogen isotope quantitative structural assessment of dominant species from the Vaccares Lagoon trophic web (Camargue Biosphere Reserve, France), *Estuarine Coastal Shelf Sci.*, *60*, 261–272.

Praetorius, S. K., and A. C. Mix (2014), Snychronization of North Pacific and Greenland climates preceded abrupt deglacial warming, *Science*, *345*, 444–448.

Pride, C., R. Thunell, D. M. Sigman, L. Keigwin, M. Altabet, and E. Tappa (1999), Nitrogen isotopic variations in the Gulf of California since the Last Deglaciation: Response to global climate change, *Paleoceanography*, *14*(3), 397–409, doi:10.1029/1999PA900004.

Rae, J. W. B., M. Sarnthein, G. L. Foster, A. Ridgwell, P. M. Grootes, and T. Elliott (2014), Deep water formation in the North Pacific and deglacial CO_2 rise, *Paleoceanography*, *29*, 645–667, doi:10.1002/2013PA002570.

Ren, H., D. M. Sigman, A. N. Meckler, B. Plessen, R. S. Robinson, Y. Rosenthal, and G. H. Haug (2009), Foraminiferal isotope evidence of reduced nitrogen fixation in the Ice Age Atlantic Ocean, *Science*, *323*, 244–248.

Ren, H., D. M. Sigman, M.-T. Chen, and S.-J. Kao (2012a), Elevated foraminifera-bound nitrogen isotopic composition during the last ice age in the South China Sea and its global and regional implications, *Global Biogeochem. Cycles*, *26*, GB1031, doi:10.1029/2010GB004020.

Ren, H., D. M. Sigman, R. C. Thunell, and M. G. Prokopenko (2012b), Nitrogen isotopic composition of planktonic foraminifera from the modern ocean and recent sediments, *Limnol. Oceanogr.*, *57*(4), 1011–1024.

Ren, H., B. G. Brunelle, D. M. Sigman, and R. S. Robinson (2013), Incorporation of trace metal in diatom frustules and its potential influence on the preservation of diatom-bound organic matter, *Mar. Chem.*, *155*, 92–101.

Robinson, R. S., and D. M. Sigman (2008), Nitrogen isotopic evidence for a poleward decrease in surface nitrate within the ice age Antarctic, *Quat. Sci. Rev.*, *27*(9–10), 1076–1090, doi:10.1016/j.quascirev.2008.02.005.

Robinson, R. S., B. G. Brunelle, and D. M. Sigman (2004), Revisiting nutrient utilization in the glacial Antarctic: Evidence from a new method for diatom-bound N isotopic analysis, *Paleoceanography*, *19*, PA3001, doi:10.1029/2003PA000996.

Saenko, O. A., A. Schmittner, and A. J. Weaver (2004), The Atlantic-Pacific seesaw, *J. Clim.*, *17*(11), 2033–2038, doi:10.1175/1520-0442(2004)017.

Sagawa, T., and K. Ikehara (2008), Intermediate water ventilation change in the subarctic northwest Pacific during the last deglaciation, *Geophys. Res. Lett.*, *35*, L24702, doi:10.1029/2008GL035133.

Sarnthein, M., H. Gebhardt, T. Kiefer, M. Kucera, M. Cook, and H. Erlenkeuser (2004), Mid Holocene origin of the sea-surface salinity low in the subarctic North Pacific, *Quat. Sci. Rev.*, *23*, 2089–2099, doi:10.1016/j.quascirev.2004.08.008.

Sarnthein, M., T. Kiefer, P. M. Grootes, H. Elderfield, and H. Erlenkeuser (2006), Warmings in the far northwestern Pacific promoted pre-Clovis immigration to America during Heinrich event 1, *Geology*, *34*(3), 141–144, doi:10.1130/G22200.1.

Schmittner, A., E. D. Galbraith, S. W. Hostetler, T. F. Pedersen, and R. Zhang (2007), Large fluctuations of dissolved oxygen in the Indian and Pacific oceans during Dansgaard-Oeschger oscillations caused by variations of North Atlantic Deep Water subduction, *Paleoceanography*, *22*, PA3207, doi:10.1029/2006PA001384.

Sedwick, P. N., and G. R. DiTullio (1997), Regulation of algal blooms in Antarctic shelf waters by the release of iron from melting sea ice, *Geophys. Res. Lett.*, *24*(20), 2515–2518, doi:10.1029/97GL02596.

Serno, S., G. Winckler, R. F. Anderson, C. T. Hayes, H. Ren, R. Gersonde, and G. H. Haug (2014), Using the natural spatial pattern of marine productivity in the Subarctic North Pacific to evaluate paleoproductivity proxies, *Paleoceanography*, *29*, 438–453, doi:10.1002/2013PA002594.

Serno, S., G. Winckler, R. F. Anderson, E. Maier, H. Ren, R. Gersonde, and G. H. Haug (2015), Comparing dust flux records from the Subarctic North Pacific and Greenland: Implications for atmospheric transport to Greenland and for the application of dust as a chronostratigraphic tool, *Paleoceanography*, *30*, 583–600, doi:10.1002/2014PA002748.

Sigman, D. M., M. A. Altabet, R. François, D. C. McCorkle, and J.-F. Gaillard (1999), The isotopic composition of diatom-bound nitrogen in Southern Ocean sediments, *Paleoceanography*, *14*, 118–134, doi:10.1029/1998PA900018.

Sigman, D. M., K. L. Casciotti, M. Andreani, C. Barford, M. Galanter, and J. K. Bohlke (2001), A bacterial method for the nitrogen isotopic analysis of nitrate in seawater and freshwater, *Anal. Chem.*, *73*(17), 4145–4153.

Sigman, D. M., S. L. Jaccard, and G. H. Haug (2004), Polar ocean stratification in a cold climate, *Nature*, *428*(6978), 59–63.

Sigman, D. M., K. L. Karsh, and K. L. Casciotti (2009), Ocean process tracers: Nitrogen isotopes in the ocean, in *Encyclopedia of Ocean Sciences*, 2nd ed., pp. 4138–4152, Elsevier, Amsterdam.

Smart, S. M., S. E. Fawcett, S. J. Thomalla, M. A. Weigand, C. J. C. Reason, and D. M. Sigman (2015), Isotopic evidence for nitrification in the Antarctic winter mixed layer, *Global Biogeochem. Cycles*, *29*, 427–445, doi:10.1002/2014GB005013.

Straub, M., M. Tremblay, D. M. Sigman, A. S. Studer, H. Ren, S. Myneni, J. R. Toggweiler, and G. H. Haug (2013a), Nutrient conditions in the subpolar North Atlantic during the last glacial period reconstructed from foraminifera-bound nitrogen isotopes, *Paleoceanography*, *28*, 79–90, doi:10.1002/palo.20013.

Straub, M., D. M. Sigman, H. Ren, A. Martínez-García, A. N. Meckler, and G. H. Haug (2013b), Glacial/interglacial changes in North Atlantic nitrogen fixation reflect excess phosphorus supply, *Nature*, *501*, 200–203.

Studer, A. S., A. Martínez-García, S. L. Jaccard, F. E. Girault, D. M. Sigman, and G. H. Haug (2012), Enhanced stratification and seasonality in the Subarctic Pacific upon Northern Hemisphere Glaciation—New evidence from diatom-bound nitrogen isotopes, alkenones and archeal tetraethers, *Earth Planet. Sci. Lett.*, *351–352*, 84–94.

Studer, A. S., K. E. Karen, S. Oleynik, D. M. Sigman, and G. H. Haug (2013), Size-specific opal-bound nitrogen isotope measurements in North Pacific sediments, *Geochim. Cosmochim. Acta*, *120*, 179–194.

Sunda, W. G., and S. A. Huntsman (1997), Interrelated influence of iron, light and cell size on marine phytoplankton growth, *Nature*, *390*, 389–392.

Takahashi, K., N. Fujitani, M. Yanada, and Y. Maita (2000), Long-term biogenic particle fluxes in the Bering Sea and the central subarctic Pacific Ocean, 1990–1995, *Deep Sea Res., Part I*, *47*, 1723–1759.

Talley, L. D., G. Pckard, W. Emery, and J. Swift (2011), *Descriptive Physical Oceanography: An Introduction*, 6th ed., pp. 1–555, Elsevier, Amsterdam.

Toggweiler, J. R., J. L. Russell, and S. R. Carson (2006), Midlatitude westerlies, atmospheric CO_2, and climate change during the ice ages, *Paleoceanography*, *21*, PA2005, doi:10.1029/2005PA001154.

Warren, B. (1983), Why is no deepwater formed in the North Pacific?, *J. Mar. Res.*, *41*, 327–347, doi:10.1029/2003GC000559.

Zheng, Y., A. Van Geen, R. F. Anderson, J. V. Gardner, and W. E. Dean (2000), Intensification of the northeast Pacific oxygen minimum zone during the Boelling-Allerod warm period, *Paleoceanography*, *15*(5), 528–536, doi:10.1029/1999PA000473.

Erratum

In the originally published version of this article, the supporting information table included biogenic flux data. The file has been replaced and this version may be considered the authoritative version of record.